BUTTERWORTH HEINEMANN

Polymer Vol. 36 No. 16, pp. 3173–3182, 1995

0032-3861/95/$10.00+0.00

Semicrystalline microfibrils and hollow fibres by precipitation with a compressed-fluid antisolvent

Gabriel Luna-Bárcenas, Sanjay K. Kanakia, Isaac C. Sanchez and Keith P. Johnston*

Department of Chemical Engineering, University of Texas, Austin, TX 78712, USA
(Received 20 July 1994; revised 1 March 1995)

Solutions of polyacrylonitrile (PAN) in dimethylformamide (DMF) sprayed into supercritical fluid carbon dioxide form hollow fibres and highly oriented microfibrils ($< 1\,\mu$m diameter). In the dilute region, microfibrils are produced with diameters as low as 100 nm due to the dipole–dipole forces, in contrast with microspheres produced from solutions of polystyrene (PS) in toluene. For PAN microfibrils, orientation increases with shear, then goes through a maximum and eventually decreases at higher flow rates due to an expanding jet. The concentration for the transition from microfibrils to a single hollow fibre is in agreement with the calculated transition concentration from the dilute to semidilute region, C^*. In the semidilute region, the morphology changes from hollow fibres to highly oriented fibrils with an increase in flow rate. The increase in turbulence enhances convective mass transport, leading to more uniform nucleation throughout the cross-section of the jet, favouring the highly oriented fibrils. The enhanced transport of CO_2 into the jet lowers the solvent quality, raising C^*, which further favours fibril formation. For both PAN–DMF and PS–toluene solutions, the transition from highly oriented microfibrils to hollow fibres occurs at about $3C^*$ (in a good solvent), suggesting some similarities in the mass-transfer pathways in each system.

(Keywords: semicrystalline microfibrils; hollow fibres; compressed-fluid antisolvent)

INTRODUCTION

There are a number of advantages in utilizing compressed CO_2 in the gaseous, liquid and supercritical fluid (SCF) states for the formation of materials with submicrometre features. Diffusion coefficients of organic solvents in SCF CO_2 are typically 1–2 orders of magnitude higher than in conventional liquid solvents. Furthermore, CO_2 is a small linear molecule that diffuses more rapidly in polymers than do other non-solvents (called antisolvents in the SCF literature). In the antisolvent precipitation process, the accelerated mass transfer in both directions can facilitate very rapid phase separation and hence the production of materials with submicrometre features. It is easy to recycle the supercritical fluid solvent at the end of the process by simply reducing the pressure. Since supercritical fluids do not have a surface tension, they can be removed without collapse of structure due to capillary forces. Drying of the product is unusually rapid. No residue is left in the product, and CO_2 has a number of desirable characteristics; for example, it is non-toxic, non-flammable and inexpensive. Furthermore, solvent waste is greatly reduced since a typical ratio of antisolvent to solvent is 30 : 1.

As an antisolvent, CO_2 has broad applicability in that it lowers the cohesive energy density of nearly all organic solvents[1–3]. In 1992, the dissertation of Dixon[4] introduced a process in which liquid solutions of polymer in solvent are sprayed into compressed carbon dioxide to form submicrometre microspheres and fibres[3,5]. In this process, so-called precipitation with a compressed-fluid antisolvent (PCA), the polymer is insoluble in CO_2, and the organic solvent is fully miscible with CO_2. It is a type of wet spinning except that the antisolvent is CO_2 instead of a liquid at ambient pressure. This concept has been used to form biologically active insulin particles ($4\,\mu$m)[6], submicrometre biodegradable poly(L-lactic acid) particles[7,8] and methylprednisolone acetate particles ($< 5\,\mu$m)[9]. Somewhat surprisingly, the particle sizes have been as small as those made by rapid expansion from supercritical solution (RESS), despite the potentially faster times for depressurization in RESS *versus* two-way mass transfer in the PCA process[10,11].

Not only can the PCA process produce polystyrene (PS) particles, but also solid and hollow fibres[3–5], highly oriented microfibrils[4,5], bicontinuous networks[4,5] and $100\,\mu$m microballoons with porous shells[4,12]. It is challenging to produce microfibrils with $1\,\mu$m and smaller dimensions by dry and wet spinning. The concept of forming fibres and microfibrils with PCA has been further demonstrated for a substituted *para*-linked aromatic polyamide (polyamide-8), a liquid-crystalline polymer, to form highly oriented 100 nm microfibrils[13].

The objective of this work is to extend the PCA process to fibre-forming semicrystalline polymers and to contrast

* To whom correspondence should be addressed

the results with those for amorphous polystyrene and the above liquid-crystalline polymer. We chose to study polyacrylonitrile (PAN), since the strong dipole–dipole interactions promote fibre formation. The fibre formation mechanism is examined as a function of the jet velocity and polymer concentration to characterize the roles of shear, solution viscosity, dilute to semidilute transitions, phase behaviour, nucleation, skin formation and mass-transfer rates and pathways. In order to understand better the results for PAN, new experiments are reported for PS over a wider range of flow rates than in our previous studies[5]. The morphologies for PS and PAN will be examined for experiments done in both dilute and semidilute organic solutions, and explained in terms of scaling-law calculations of the transition concentration between these two regions.

THEORY

Scaling-law theory of C*

In the dilute regime, polymer chains behave as independent entities. In the semidilute region, the chains are capable of entangling with one another. The threshold region at which overlap starts would be expected to occur when the total volume of the chains just fills the available volume[14]. Here the concentration C^* is comparable to that in the polymer coil[15]. Predictions of scaling-law theory, for polymers of high (infinite) molecular weight in both good solvent and Θ solvent in the semidilute region, are shown in *Table 1*.

The scaling-law expression for C^* is:

$$C^* \sim N/R_g^3 \tag{1}$$

where N is the degree of polymerization and R_g is the radius of gyration. The ratio of C^* in a good solvent to that in a Θ solvent is:

$$C^*(\text{good})/C^*(\Theta) \sim N^{0.3} \tag{2}$$

In the PCA process the polymer starts in a good solvent. As CO_2 diffuses into the solution and the solvent diffuses out, the binary CO_2–solvent mixture becomes a progressively poorer solvent. Consequently, R_g decreases such that a higher C^* is required for overlap of the chains.

Theory of polymer precipitation with a compressed-fluid antisolvent

The mechanism of fibre formation is complex as it involves hydrodynamics, phase equilibria, two-way mass transfer, nucleation and crystallization[16]. To provide a basis for understanding the experimental results, we present a summary of the relevant phase behaviour and the mass-transfer pathways[3,17–19]. *Figure 1* shows schematically a phase diagram for a ternary system consisting of a semicrystalline polymer, an organic solvent and a compressed-fluid antisolvent. This diagram shows (i) a stable region, located between the solvent–polymer axis and the binodal (coexistence) curve, (ii) a metastable region, located between the binodal and spinodal curves, and (iii) an unstable region, located inside the spinodal curve. The binodal and spinodal coincide at the plait point or the critical point. For a binary polymer–solvent mixture, the transition concentration C^*, which divides the dilute and the semidilute regimes, is near the critical point[15]. For a polymer–solvent–antisolvent ternary system, C^* will increase with the ratio of antisolvent to solvent.

Table 1 Scaling-law predictions in the semidilute regime (from Napper[14])

	Scaling law	
Property	Good solvent	Θ solvent
$R_g \sim$	$N^{3/5}$	$N^{1/2}$
$C^* \sim$	$N^{-4/5}$	$N^{-1/2}$

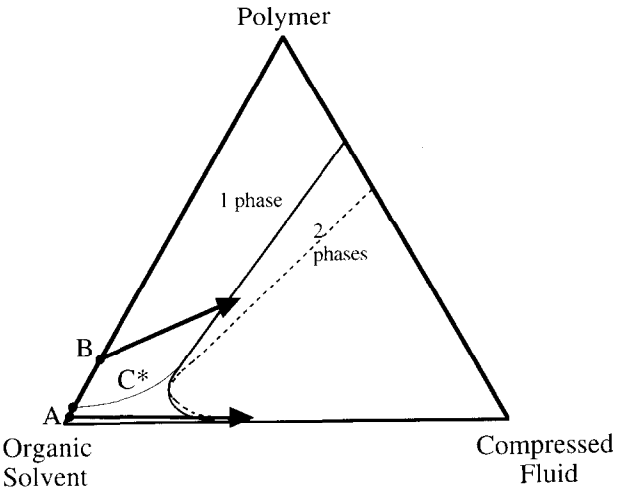

Figure 1 Schematic ternary phase diagram showing different precipitation pathways with a compressed-fluid antisolvent: (——) binodal curve; (- - - -) spinodal curve; (——) C* curve

The morphology is determined to a large extent by the mass-transfer pathway on the phase diagram. If the polymer composition in the metastable region at the point of phase separation is smaller than the plait point (mass-transfer pathway A), the polymer-rich phase will nucleate and grow in a solvent-rich continuous phase. In pathway B, the opposite holds for nucleation and growth of the solvent-rich phase in a polymer-rich continuous phase. In either case, the pathway can cross the spinodal line, where further phase separation is by spinodal decomposition. For a semicrystalline polymer, crystallization helps to preserve microstructures with high surface area, which can otherwise coarsen to lower the free energy. The location of the crystallization curve relative to the plait point has been considered previously[20], but is unknown for the polyacrylonitrile–dimethylformamide–CO_2 (PAN–DMF–CO_2) system.

At low polymer concentrations (pathway A), amorphous PS[3] and semicrystalline poly(L-lactic acid)[7] microspheres have been produced on the order of 100 nm–1 μm. In contrast, liquid-crystalline polymers, such as a polyamide-8, produce highly oriented microfibrils at dilute polymer concentrations[13], illustrating the importance of fibre-forming interactions. In pathway B, hollow fibres have been formed with porous shells and thin skins[5,19]. When the mass-transfer pathway is near the plait point (not shown) where the spinodal is close to the binodal, phase separation is governed primarily by spinodal decomposition. In this region, bicontinuous interconnected networks of polymer and solvent voids have been formed, as well as highly oriented microfibrils[5].

The mechanism of jet break-up can be predicted for Newtonian fluids as a function of the Reynolds number (N_{Re}) and Weber number (N_{We})[21]. The latter is the ratio of the inertial forces to surface tension forces and is given by:

$$N_{We} = \rho_A U^2 D/\sigma \quad (3)$$

where ρ_A is the antisolvent density, U is the relative velocity, D is the jet diameter and σ is the interfacial tension. If N_{We} is large, the deforming inertial forces are large compared to the re-forming surface forces. The Ohnesorge number N_{Oh} is defined by:

$$N_{Oh} = N_{We}^{1/2}/N_{Re} = \eta/(\rho D\sigma)^{1/2} \quad (4)$$

where η is the solution viscosity. At high values of N_{Oh} and N_{Re}, the jet breaks up by atomization. At low values of N_{Oh} and N_{Re}, the jet break-up results from Rayleigh instabilities[21]. Therefore, higher velocities favour atomization. Because σ is small between the polymer solution and CO_2 (when the polymer is dilute), Rayleigh instabilities are unlikely.

EXPERIMENTAL

Polyacrylonitrile (PAN) (Aldrich Chemical Co. Inc., $M_w = 150\,000$) and *N*,*N*-dimethylformamide (DMF) (Fisher Scientific, ACS grade) were used as received. Polymer concentrations from 0.05 to 0.5 wt% were sprayed through a 50 μm internal diameter (i.d.) by 18 cm long fused silica capillary tube, which had a polyimide coating. Concentrations from 1.0 to 2.5% were sprayed through a 50 μm i.d. by 2.5 cm long capillary tube. The 4.0% polymer solution was sprayed through a 100 μm i.d. by 2.5 cm long capillary tube. The diameter and length were varied depending on the solution viscosity.

Polystyrene (Pressure Chemicals, $M_w = 200\,000$) in toluene (Fisher, ACS grade) solutions were studied from 5 to 10%. For this range of compositions, the solutions were sprayed through a 50 μm i.d. by 2.5 cm long capillary tube.

The experimental apparatus in *Figure 2* is similar to a previous design[4]. The spray vessel consisted of a 13 ml sapphire tube (3.175 cm o.d. × 1.27 cm i.d. × 10.16 cm long). Both the spray and the precipitation were viewed. To facilitate recovery of the precipitated polymer, a 0.2 μm cellulose filter (Micron Separations Inc.) was inserted between the two stainless-steel screens at the bottom of the cell.

The system was equilibrated for 15–20 min, and then the polymer solution was sprayed for short times (~ 5–10 s). In all cases, the DMF was miscible with the CO_2 and a second solvent phase did not form. At lower temperatures from 0 to 20°C, a meniscus formed, indicating phase separation, which is consistent with previous studies[13]. Therefore, experiments at low temperatures were not performed. After spraying, more CO_2 was flowed through the system to dry the precipitated polymer while maintaining a constant pressure and temperature. After 20–30 min of purging with CO_2, the system was slowly depressurized over a 20–30 min period at constant temperature. For all the PAN experiments done in the present study, the temperature was set to 40°C and the pressure to 103 bar, so that $\rho = 0.66\,g\,ml^{-1}$. At this condition, CO_2 is above its critical point ($T_c = 31.05$°C, $P_c = 73.8$ bar).

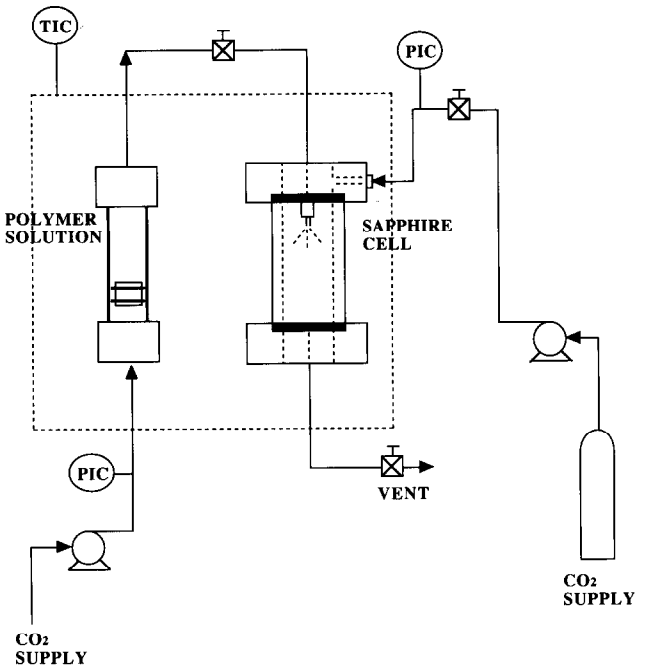

Figure 2 Apparatus for precipitation of polymer fibrils and fibres with a compressed-fluid antisolvent (TIC = temperature indicator and controller, PIC = pressure indicator and controller)

The products were analysed with a scanning electron microscope (SEM). A portion of the sample was mounted on a piece of double-stick carbon tape, attached to a 3/8 inch × 3/8 inch (~ 1 cm × 1 cm) brass SEM cylinder, sputter-coated with gold–palladium, and imaged in a SEM (JEOL JSM-35C).

Before spraying a given polymer solution into CO_2, solution flow rate *versus* pressure drop measurements were done to determine the solution viscosity. The solution flowed into a small vial at ambient pressure. The amount of polymer solution collected in a given time period was weighed to within 0.0001 g. Three replicate experiments were made for each polymer solution and the flow rate was averaged. Given the flow rate *versus* pressure drop, the non-Newtonian viscosity was calculated by using the Weissenberg–Rabinowitsch equation, neglecting end effects[22].

RESULTS AND DISCUSSION

Viscosity measurement

The viscosity is calculated at the capillary wall (η_R; $g\,cm^{-1}\,s^{-1}$) and is given as a function of shear rate ($\dot{\gamma}_R$, s^{-1}) in *Figure 3* over a wide concentration range at 40°C. At very dilute polymer concentrations (0.05 and 0.1%) Newtonian behaviour is observed. As the concentration increases, the viscosity increases significantly, and shear-thinning behaviour is observed as a function of shear rate.

Dilute region: low shear

Solutions of PAN in DMF from 0.05 to 1% are in the dilute region as shown below. The temperature and density of CO_2 were held constant at 40°C and $0.66\,g\,ml^{-1}$, respectively, for all of the PAN experiments

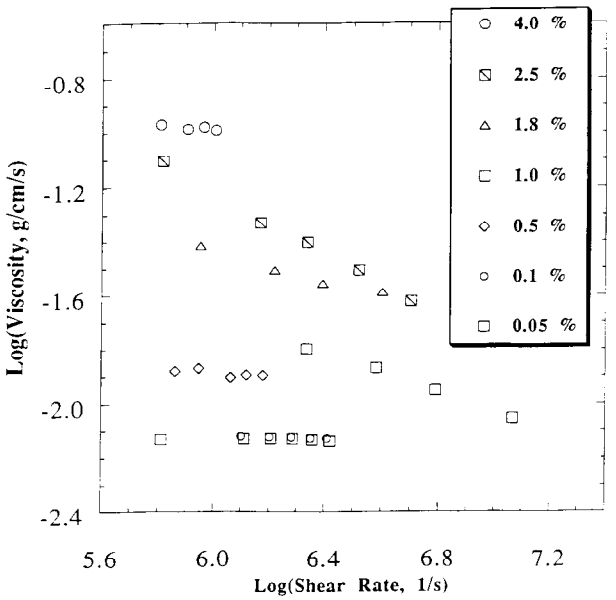

Figure 3 Non-Newtonian viscosity at the capillary wall as a function of shear rate and PAN concentration in DMF (40°C)

in this study. Over this concentration range, highly oriented microfibrils with diameters from 100 to 200 nm are formed for the flow rates studied (see *Figure 4*). In *Figure 4a* the polymer solution flow rate was $0.36\,\mathrm{ml\,min^{-1}}$. During the spray into CO_2, it was observed that the jet broke up into two or three parts. The polymer precipitated in these separated streams about 1–2 cm away from the tip of the nozzle. Further away from the nozzle, the particles coalesced. Because the concentration of the polymer was low, the resulting microfibrils were not thick or viscous enough to form a single continuous fibre. Instead, light airy bundles of microfibrils landed on top of each other at the bottom of the sapphire tube. The diameter of a typical bundle was ~ 100–$200\,\mu\mathrm{m}$ and the length was about the same.

For the same CO_2 conditions, similar microfibrils were produced for polymer concentrations up to 1% as shown in *Figures 5* and *6* and *Table 2*. For this range of concentrations, it will be shown that the polymer solution is in the dilute regime based on the calculated C^* and the morphologies produced. For the flow rates studied, the lowest viscosity was 0.73 cP for a 0.05% polymer concentration, and the highest was 1.6 cP for a 1.0% polymer concentration. This change was too small to have much effect on the morphology.

At similar conditions, microspheres and not microfibrils are formed for amorphous PS in toluene[3] and semicrystalline poly(L-lactic acid) in methylene chloride[7]. Therefore, the strong intermolecular forces between the nitrile dipoles in PAN are responsible for the fibril formation. Upon close inspection, a number of beads are present on the microfibrils, suggesting that the polymer phase is the discrete phase, as expected for these dilute concentrations. A similar morphology is obtained for 0.03 and 0.09% polyamide-8 in DMF solutions, due to the liquid-crystalline domains, which favour fibre formation[13]. For polyamide-8, it is unknown if this morphology can be formed at higher, more practical, concentrations.

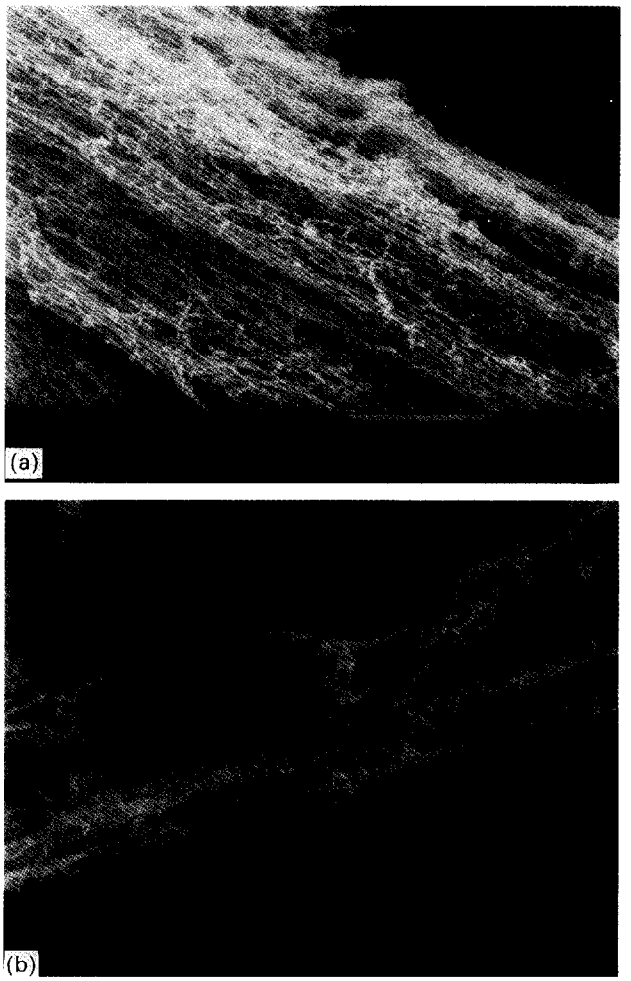

Figure 4 SEM micrographs of PAN fibrils formed by spraying a 0.05% PAN in DMF solution through a $50\,\mu\mathrm{m}$ i.d., 18 cm long nozzle into CO_2 at 40°C, $0.66\,\mathrm{g\,ml^{-1}}$: (a) $0.36\,\mathrm{ml\,min^{-1}}$; (b) $1.5\,\mathrm{ml\,min^{-1}}$

Dilute region: effect of shear

To examine the effect of shear on morphology, experiments were performed at higher solution flow rates. A few representative examples are shown in *Figures 4b* and *5d* for 0.05 to 0.5% solutions. Again, microfibrils are formed at each condition. In *Figure 4b* for a 0.05% solution with a flow rate of $1.5\,\mathrm{ml\,min^{-1}}$, the microfibrils are more spread apart than those formed at $0.36\,\mathrm{ml\,min^{-1}}$ (*Figure 4a*). Based on *Figure 3*, the viscosity is constant over this range in shear rate. The spreading of the microfibrils is due to an expanding jet. It was observed visually that the jet became wider at this higher flow rate.

Similar behaviour was observed for a 0.5% solution, which was sprayed at three different flow rates. Owing to the higher polymer concentration, enough sample for SEM could be obtained at even lower flow rates. *Figure 5c* shows results for a low flow rate of $0.2\,\mathrm{ml\,min^{-1}}$ ($\dot{\gamma}_R = 7.3 \times 10^5\,\mathrm{s^{-1}}$, $\eta_R = 0.14\,\mathrm{g\,cm^{-1}\,s^{-1}}$). The microfibrils are no longer aligned in the jet direction, because the shear in the capillary is too weak to orient the microfibrils. At an intermediate flow rate of $0.5\,\mathrm{ml\,min^{-1}}$ ($\dot{\gamma}_R = 9 \times 10^5\,\mathrm{s^{-1}}$, $\eta_R = 0.013\,\mathrm{g\,cm^{-1}\,s^{-1}}$), highly oriented microfibrils are produced (*Figure 5a*). Here, the shear rate is approximately 23% greater. At a

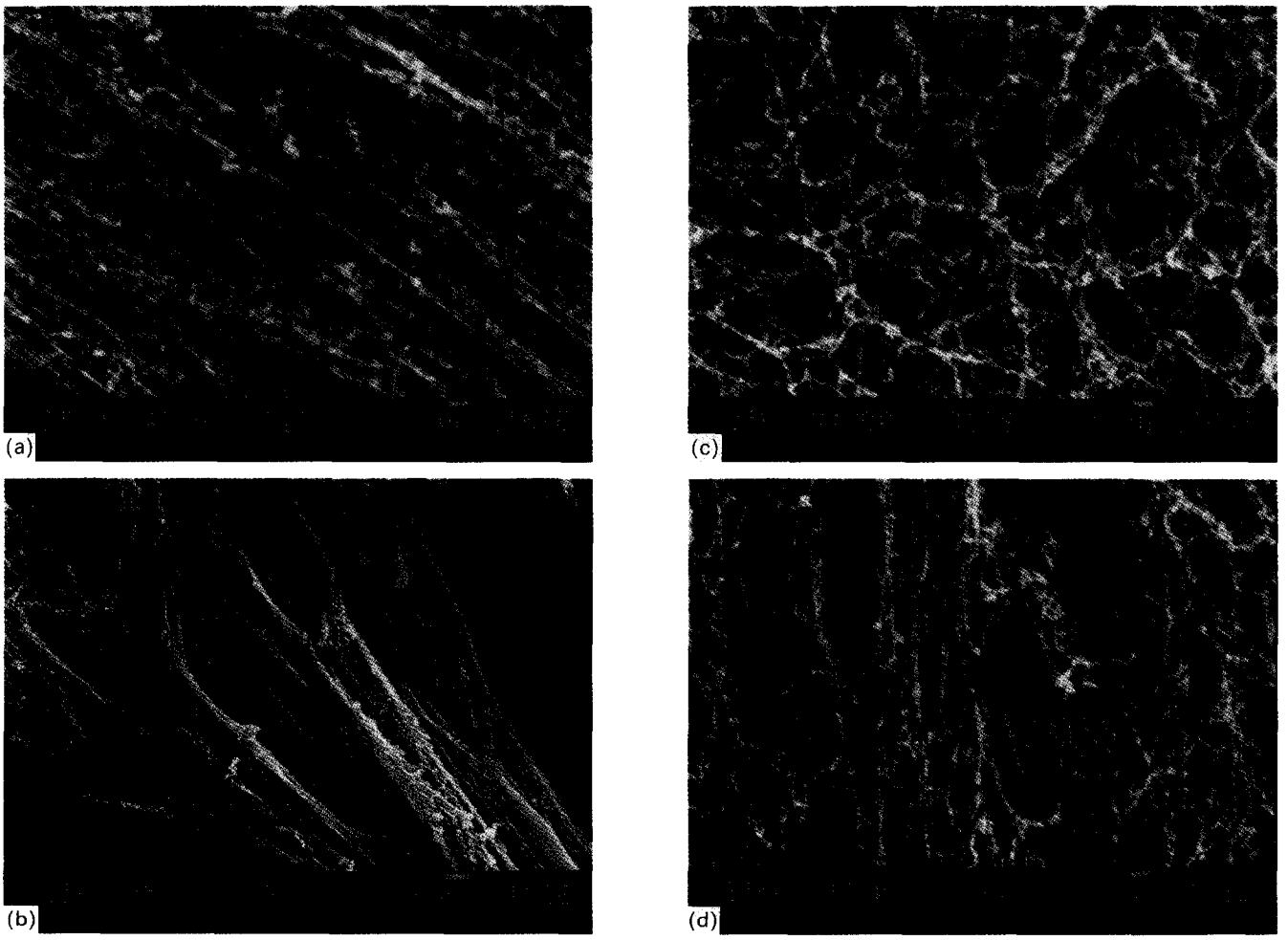

Figure 5 SEM micrographs of PAN fibrils formed by spraying a 0.5% PAN in DMF solution through a 50 μm i.d., 18 cm long nozzle into CO_2 at 40°C, 0.66 g ml^{-1}: (a) 0.5 ml min^{-1}; (b) detail of (a); (c) 0.2 ml min^{-1}; (d) 1.0 ml min^{-1}

Figure 6 SEM micrograph of PAN fibrils formed by spraying a 1% PAN in DMF solution through a 50 μm i.d., 2.5 cm long nozzle into CO_2 at 40°C, 0.66 g ml^{-1}: flow rate, 0.7 ml min^{-1}

high flow rate of 1.0 ml min^{-1} ($\dot{\gamma}_R = 1.5 \times 10^6$ s^{-1}, $\eta_R = 0.012$ g cm^{-1} s^{-1}) (*Figure 5d*), the orientation along the jet flow is somewhat distorted and the distance between microfibrils is higher, as was observed above for the 0.05% concentration. For each flow rate, the fibres are about 5 mm long, in contrast with the 0.1 mm long fibres for the lower concentrations, illustrating the effects of higher viscosity and entanglement during phase separation.

A control experiment at the same conditions was performed with water as the antisolvent at 40°C. A 1% PAN in DMF solution was sprayed into water at a flow rate of 0.7 ml min^{-1}. Single porous fibres with an average diameter of 10 μm were formed without any subfibres (microfibrils) (see *Figure 7*). This comparison illustrates the more rapid phase-separation mechanism for a compressed-fluid antisolvent, compared with a liquid solvent. The differences in the results may not be attributed to differences in solvent–antisolvent interactions, since DMF is highly soluble in both CO_2 and water.

We now present a mechanism to explain the effect of shear on the formation of microfibrils. At low shear rates, random coils slip through the solvent without being deformed by the velocity gradient. At higher shear rates the coils are elongated by shear and the viscosity decreases. Here, the microfibrils are highly oriented in the axial direction, suggesting that the polymer nucleates while the coils are still elongated. Because diffusion is higher in both directions for CO_2 as an antisolvent,

Table 2 Polymer morphologies produced by spraying a solution of PAN in DMF into CO_2 at 40°C ($\rho_{CO_2} = 0.66\,g\,ml^{-1}$)[a]

Polymer conc. (wt%)	Solution flow rate ($ml\,min^{-1}$)	Nozzle length (cm)	Macrostructure	Microstructure (SEM)
0.05	0.16	18	Fibre bundles, 100–200 μm	Randomly oriented microfibrils, 100 nm diameter
0.05	0.36	18	Fibre bundles, 100–200 μm	Highly oriented microfibrils, 100 nm diameter
0.05	1.51	18	Fibre bundles, 100–200 μm	Oriented expanded microfibrils, 100 nm diameter
0.1	0.13	18	Fibre bundles, 100–200 μm	Randomly oriented microfibrils, 100 nm diameter
0.1	0.6	18	Fibre bundles, 100–200 μm	Highly oriented microfibrils, 100 nm diameter
0.1	1.6	18	Fibre bundles, 100–200 μm	Oriented expanded microfibrils, 100 nm diameter
0.5	0.2	18	Fibre bundles, ~ 200 μm diameter, ~ 5 mm long	Randomly oriented microfibrils, 100 nm diameter
0.5	0.5	18	Fibre bundles, ~ 200 μm diameter, ~ 5 mm long	Highly oriented microfibrils, 100 nm diameter
0.5	1.0	18	Fibre bundles, ~ 200 μm diameter, ~ 5 mm long	Oriented expanded microfibrils, 100 nm diameter
1	0.7	2.5	Fibre bundles, ~ 0.5 mm diameter, ~ 1 cm long	Highly oriented microfibrils, 100 nm diameter
1	2.0	2.5	Fibre bundles, ~ 0.5 mm diameter, ~ 0.1–0.5 cm long	Randomly oriented microfibrils, ≤ 1 μm
1[b]	0.7	2.5	Fibre bundles, ~ 0.5 mm diameter, ~ 2–3 cm long	Porous fibre, ~ 10 μm diameter
1.8	0.2	2.5	Fibre, 20 μm diameter, ~ 3–4 cm long	Fiber, ~ 10–15 μm diameter
1.8	2.0	2.5	Fibre, ~ 2–3 cm long	Oriented fibrils, ~ 1–2 μm diameter
2.5	0.36	2.5	Solid fibre, many cm long	Hollow fibre, ~ 25 μm diameter
2.5	2.0	2.5	Fibre, 2–3 cm long	Oriented fibrils, ~ 1–2 μm diameter
4[c]	0.7	2.5	Fibre, many cm long	Hollow porous fibre, 1:2 aspect ratio
4[c]	1.5	2.5	Fibre, many cm long	Hollow porous fibre, 120 μm diameter

[a] Unless otherwise noted, the solution was sprayed through a 50 μm i.d. nozzle
[b] Sprayed into liquid water at 40°C
[c] Solution sprayed through a 100 μm i.d. nozzle

Figure 7 SEM micrograph of PAN fibres formed by spraying a 1% PAN in DMF solution through a 50 μm i.d., 2.5 cm long nozzle into water at 40°C and atmospheric pressure: flow rate, 0.7 $ml\,min^{-1}$

relative to a conventional liquid, nucleation can be especially rapid. The formation of many nuclei favours the production of a large number of very small microfibrils. Furthermore, nucleation rates can be orders of magnitude faster for extended coils relative to random coils[23]. With fast nucleation rates, the microfibrils can be formed in the jet before the coils undergo much relaxation. The rapid drying of the microfibrils due to rapid diffusion of solvent out of the jet helps to prevent coarsening of the microfibrils during solidification.

It is possible that the free jet experiences elongational flow, if CO_2 diffuses in faster than DMF diffuses out[16]. This extra elongation, in addition to that caused by shear in the capillary, would further orient the microfibrils.

The jet break-up mechanism may be examined in terms of N_{Re} and N_{Oh}. High values of these two numbers favour atomization over Rayleigh instabilities. The ratio of various dimensionless numbers is given in *Table 3* for two flow rates, assuming a constant σ. As the flow rate increases, N_{Oh} changes little, while N_{Re} increases by a factor of about 6. The spreading of the fibrils is caused by the turbulence generated in the jet by interactions with the CO_2 fluid phase. A high N_{Re} of 28 000 is calculated for the CO_2 fluid phase for the highest flow rate (see *Table 3*). It is likely that the expanding jet is due in part to Kelvin–Helmholtz instabilities. In conclusion, as the flow rate is increased, orientation increases with shear, then goes through a maximum, and eventually decreases due to an expanding jet.

Table 3 Change in Reynolds, Weber and Ohnesorge numbers with flow rate for a solution of 0.5% PAN in DMF sprayed into CO_2 at 40°C ($\rho_{CO_2} = 0.66\,g\,ml^{-1}$)[a]

Q ($ml\,min^{-1}$)	U ($cm\,s^{-1}$)	μ ($g\,cm^{-1}\,s^{-1}$)	N_{Re}	$\frac{N_{Re}}{N_{Re}(Q=0.2)}$	$\frac{N_{We}}{N_{We}(Q=0.2)}$	$\frac{N_{Oh}}{N_{Oh}(Q=0.2)}$
0.2	170.0	0.0140	57	–	–	–
0.5	424.4	0.0130	153	2.7	6.3	0.94
1.0	849.0	0.0120	334	5.8	25	0.86

[a] $\rho_{solution} = 0.944\,g\,ml^{-1}$; nozzle i.d. = 50 μm, length = 2.5 cm

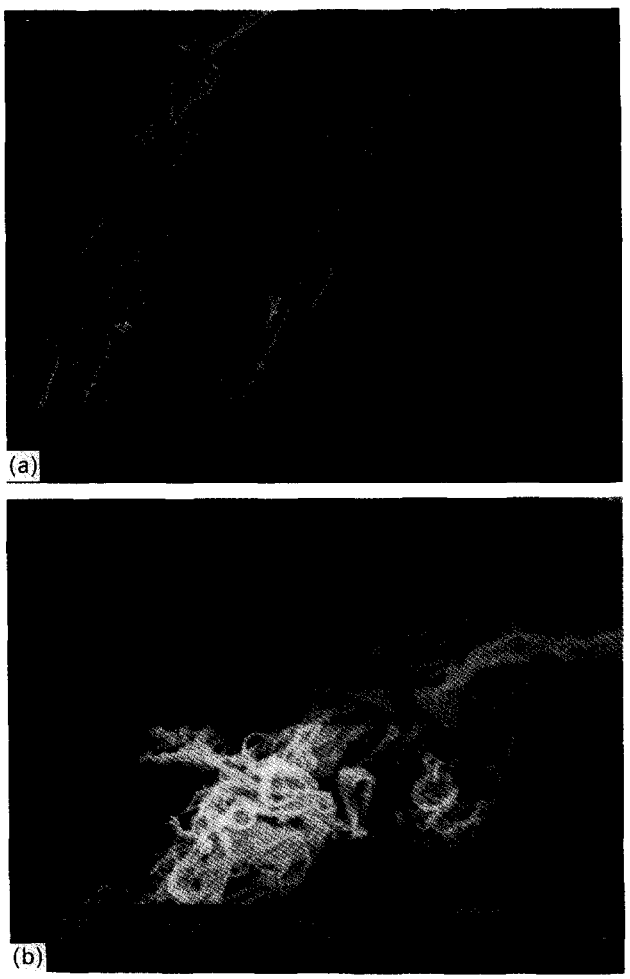

Figure 8 SEM micrographs of PAN fibrils formed by spraying a 1.8% PAN in DMF solution through a 50 μm i.d., 2.5 cm long nozzle into CO_2 at 40°C, 0.66 $g\,ml^{-1}$: (a) 0.2 $ml\,min^{-1}$; (b) 2.0 $ml\,min^{-1}$

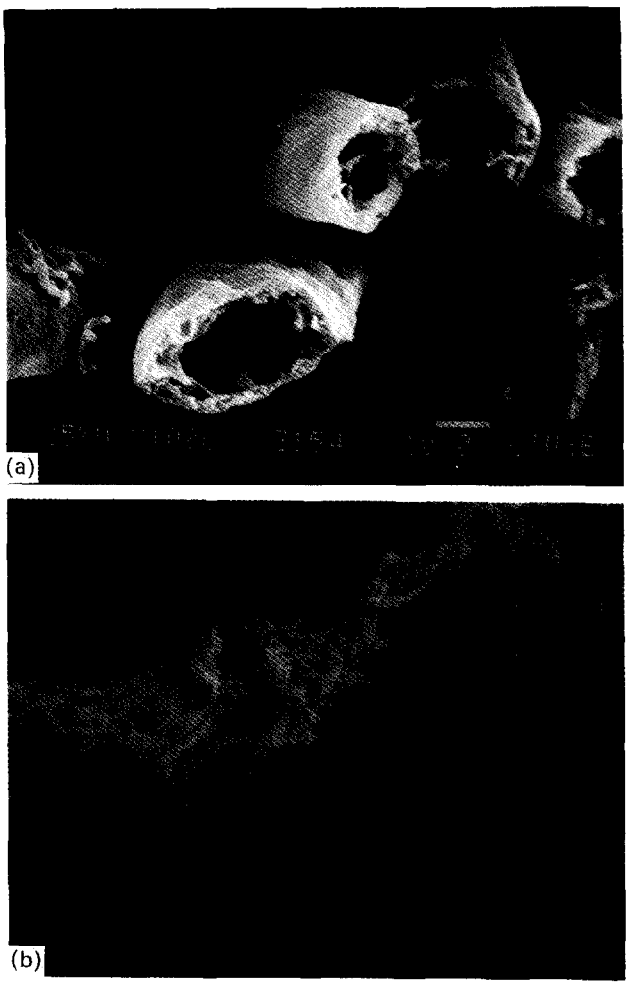

Figure 9 SEM micrographs of PAN fibres formed by spraying a 2.5% PAN in DMF solution through a 50 μm i.d., 2.5 cm long nozzle into CO_2 at 40°C, 0.66 $g\,ml^{-1}$: (a) 0.36 $ml\,min^{-1}$; (b) 2.0 $ml\,min^{-1}$

Semi-dilute region: low shear

In the semidilute region, it may be expected that chain entanglement and increased solution viscosity influence the morphology of the fibres. The N_{Re} is reduced and it was observed that the jet no longer breaks up in the spray. Increasing the polymer concentration above 1% leads to long continuous fibres. For a composition of 1.8% and flow rate of 0.2 $ml\,min^{-1}$, ~ 3 cm long fibres are formed, with diameters of 10–15 μm (*Figure 8a*). These fibres are not uniform, but are composed of 2–5 μm fibrils.

A variety of factors contribute to the change in morphology from the dilute to semidilute region. As the mass-transfer pathways move upwards to higher polymer concentrations, the volume fraction of polymer in the resulting macroscopic fibre increases. The pathway shifts from polymer-discrete towards polymer-continuous morphologies. Because the jet does not break up, the mass-transfer distances are longer and nucleation is slower. Also diffusion is slower in both directions owing to the higher viscosities in the liquid phase. It becomes harder to shear the polymer coils to form oriented chains. This will further slow down nucleation[23]. Consequently, the fibril diameters are larger and the fibre lengths increase.

Increasing the polyacrylonitrile composition to 2.5% for a flow rate of 0.36 $ml\,min^{-1}$ produces a single hollow fibre. The jet did not break up and became cloudy due to precipitation about 1 cm down from the tip of the nozzle.

The fibre was immersed in liquid nitrogen and cut with a razor blade to obtain a micrograph of the cross-section of the fibre. The fibre has a well defined cylindrical shape (*Figure 9a*) with a diameter of about 25 μm and shell thickness ranging from 3 to 5 μm. The hollow fibre has a dense skin that is formed during solvent loss from the outermost region of the jet[5,19,24].

The mechanism for hollow-fibre formation in the PCA process has been discussed previously[5]. In the semidilute region, it is likely that the mass-transfer pathway crosses the binodal curve on the polymer-rich side of the phase diagram (see *Figure 1*). In the jet, the skin (barrier) forms rapidly and restricts the outward diffusion of DMF. The diffusion of CO_2 through this skin is faster than that of the solvent, because of its small size[25]. As more CO_2 diffuses into the jet, the phase-separation interface between polymer and solvent moves towards the centre. The interior remains rich in solvent, allowing the CO_2-rich voids to grow. Thus, the porosity is non-uniform, and the pores become larger from the skin towards the inside. These voids coalesce and with sufficient time before vitrification a hollow structure is produced, as observed.

For a 4.0% solution with a solution flow rate of 0.7 ml min^{-1} ($\dot{\gamma}_R = 6.31 \times 10^5$, $\eta_R = 0.110$ g cm^{-1} s^{-1}), hollow fibres are again formed (*Table 2*). Because of the larger polymer concentration, the shell is much thicker than in a 2.5% concentration, since the mass-transfer pathway shifts upwards. The higher viscosity also contributes to the thicker shell by hindering growth and coalescence of the voids.

Semidilute region: effect of shear

Based on the above results, a transition from polymer-discrete to polymer-continuous morphology occurs for an initial polyacrylonitrile composition between 1.0% and 2.5%. We now discuss the effect of shear on morphology in this transition region. In the semidilute region, interpenetration of polymer coils causes kinetic limitations for chain orientation due to shear. Whereas shear may be expected to favour highly oriented fibrils, it will produce somewhat less orientation than in the dilute region, as observed. A rather significant change in microstructure occurs at 1.8% as the flow rate is increased from 0.2 ml min^{-1} (*Figure 8a*) to 2 ml min^{-1} (*Figure 8b*). The fibrils become considerably smaller (1–3 μm) and less oriented owing to the turbulence in the jet. The spreading of the fibrils is even greater than in *Figure 8a*, probably due to the higher flow rate. The shear rate increases about 260%, reducing the viscosity by 33%. The fibril diameters in *Figure 8b* are comparable to those for 10% PS in toluene[5].

In order to define the transition region further, a high shear rate ($\dot{\gamma}_R = 2.50 \times 10^6$ s^{-1}, $\eta_R = 0.037$ g cm^{-1} s^{-1}) was studied for a 2.5% polymer solution (*Figure 9b*). The shear rate was increased about 280% and the viscosity was reduced by 53% when the low flow rate was increased from 0.36 to 2.0 ml min^{-1} (*Figure 9b*). Similar changes are observed as for the 1.8% experiments. The fibril diameters are still small, i.e. 1–3 μm.

The increase of the solution flow rate can significantly reduce the chain entanglement and thus the viscosity. Higher flow rates enhance turbulence and convective mass transfer in the jet. Consequently, nucleation occurs more uniformly throughout the cross-section of the jet, and not just as the outer surface. Instead of forming a single fibre with a skin, many small-diameter fibrils are produced. The orientation of the polymer chains leaving the capillary further facilitates this nucleation. It is not obvious whether the curvature of the fibrils indicates growth of a polymer-discrete or polymer-continuous phase. It is conceivable that much of the phase separation is by spinodal decomposition, given the large surface area of the fibrils. Because the concentration is near the plait point, the metastable nucleation and growth region is relatively narrow (see *Figure 1*). The rapid mass transfer reduces the time in the growth region, and when the spinodal is crossed a large number of fibrils are formed.

For a concentration of 4%, it was no longer possible to form small fibrils (see *Table 2*). The flow rate was increased from 0.7 to 1.5 ml min^{-1}. The solution viscosity decreased about 18% and the shear rate increased approximately 60% ($\dot{\gamma}_{Re} = 1.02 \times 10^6$ s^{-1}, $\eta_R = 0.090$ g cm^{-1} s^{-1}) when compared to the lower flow rate (see *Table 2*). Here the higher viscosity and entanglement reduce orientation of polymer chains in the capillary and reduce mass-transfer rates. Both of these factors slow down nucleation in the interior of the jet, and skin formation occurs before the fibrils form. The fibre is still porous and hollow, and the higher concentration leads to a much higher diameter of 120 μm. Thus, the mass-transfer pathway is in the polymer-continuous region. The increase in the diameter relative to the capillary diameter may be due to inward diffusion of CO_2. It is known that CO_2 diffuses faster through a polymer skin than does a larger liquid molecule.

Two techniques were used to measure the crystallinity of the fibrils produced in the semidilute region. A matted sample of the fibrils was analysed with a wide-angle X-ray diffractometer using copper K_α radiation and equipped with a diffracted beam monochromator. Also, a single fibre was mounted in a photographic flat-plate diffractometer. Similar results were obtained with each technique. The X-ray diffraction patterns contain two broad bands indicating short-range order on a scale less than 10 Å. The *d* spacings were 10.6 Å and 3.4 Å. There is no regularity from unit cell to unit cell, indicating very small crystallites. Therefore, larger crystalline domains are not required to form fibrils in the semidilute region.

Influence of C^* *on morphology*

The change in morphology from oriented fibrils to a single fibre is expected to be influenced by the large increase in entanglement above C^*. The C^* in DMF, which is a good solvent for PAN, may be determined from the intrinsic viscosity $[\eta]$, i.e. $C^* \sim [\eta]^{-1}$ (ref. 26). The value of $[\eta]$ (ml g^{-1}) may be calculated from the Mark–Houwink equation:

$$[\eta] = KM^a \tag{5}$$

where K and a are constants. Allcock and Lampe[27] reported values of $K = 2.33 \times 10^{-2}$ and $a = 0.75$ for the system PAN–DMF at 25°C. For $M = 150\,000$, these values lead to C^* (good) $\sim 0.6\%$. By using equation (2), $C^*(\Theta) \sim 6\%$.

As shown above in *Figure 1*, C^* changes with solvent composition. As CO_2 diffuses into the jet and the solvent

diffuses out, R_g decreases and C^* increases. In the flowing jet, the mass-transfer pathway may reach the phase boundary before the mixed solvent becomes a Θ solvent. The following suggests that this is indeed the case. As shown in *Table 2*, a transition from polymer-discrete to polymer-continuous morphologies occurs at a polymer concentration of about 1.8%. This change in morphology is expected to take place at C^* where the chains become entangled. Thus, it appears that phase separation took place at a point where C^* was intermediate between the good-solvent and Θ-solvent limits.

It is possible that a dynamic effect on C^* may influence the morphology. At higher flow rates, shear aligns the chains such that higher polymer concentrations are required for overlap (C^* increases). The higher orientation of the chains and reduced entanglement favour a transition from single fibre to many small fibrils. This transition is due primarily to higher mass-transfer rates, which cause more uniform nucleation throughout the jet, but this additional dynamic effect on C^* may also be present.

Polystyrene: semidilute region (effect of shear)

To understand further the results for PAN in the semidilute region, we have performed experiments for amorphous PS in toluene to complement an earlier study[4,5]. Specifically, we examine a much wider range of flow rates to study the effects of shear. These results should shed light on the PAN studies, since the amorphous PS system is simpler.

For an initial polystyrene composition of 5% and a CO_2 density of $0.94\,g\,ml^{-1}$, a hollow cylindrical fibre is observed, as shown in *Figure 10a* and *Table 4*. The flow rate is approximately $0.1\,ml\,min^{-1}$. The continuous hollow fibre is many centimetres long, with an average diameter of 100 μm. Here the viscosity is just enough to hold the fibre together, hindering jet break-up, according to comparison with previous results[5]. This diameter is twice as large as the nozzle inside diameter. Again, this is due in part to the faster mass-transfer rate of CO_2 into the liquid jet relative to the toluene rate out. Also, viscoelastic forces cause some die swell to occur. The shell thickness is of the order of 2 μm and it contains submicrometre pores and a skin. Upon careful inspection of *Figure 10a*, small microspheres of the order of 2–3 μm are present inside the hollow fibre. Thus, it is likely that the transition from dilute to semidilute region occurs close to this concentration. Polymer-discrete microspheres are characteristic of the dilute region, while polymer-continuous hollow fibres are characteristic of the semidilute region.

At a higher solution flow rate of $3.3\,ml\,min^{-1}$, continuous fibres are also observed; however, the microstructure is significantly different (*Figure 10b*). These fibrils, which are of the order of 1–3 μm, are comparable in diameter to that of the microparticles observed within the hollow fibre shown in *Figure 10a*. As explained above, the reduced viscosity and higher N_{Re} increase turbulence in the jet and mass-transfer rates, facilitating fibril formation. A manifestation of the higher solution flow rate is that the small particles inside the fibre in *Figure 10a* are stretched and coalesce to form fibrils. A transition from small particles to fibrils with an increase in flow rate has also been observed before[5].

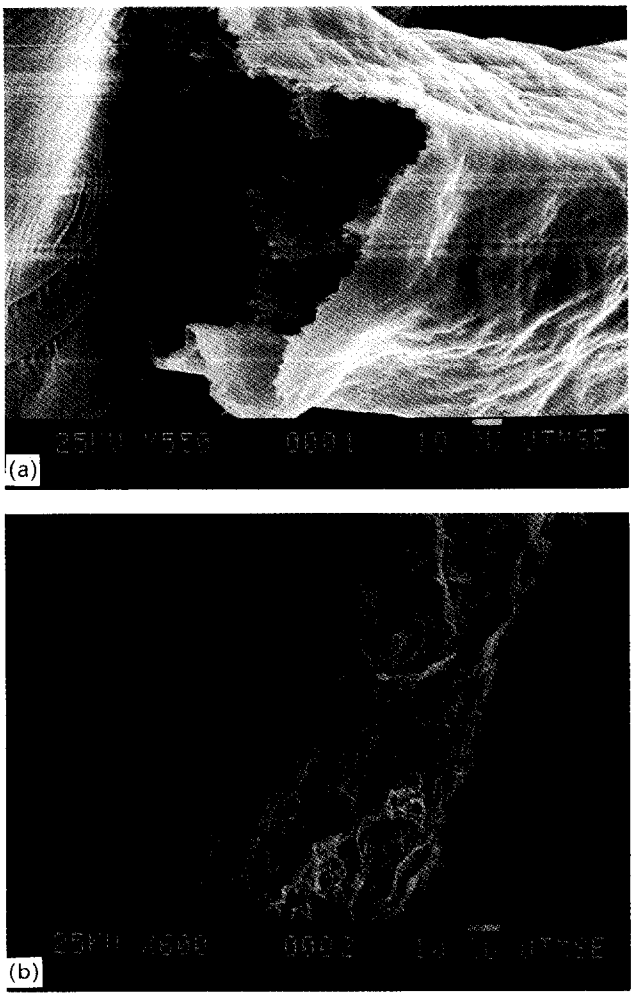

Figure 10 SEM micrographs of polystyrene fibres formed by spraying a 5% polystyrene in toluene solution through a 50 μm i.d., 2.5 cm long nozzle into CO_2 at 0.4°C, $0.94\,g\,ml^{-1}$: (a) $0.1\,ml\,min^{-1}$; (b) $3.3\,ml\,min^{-1}$

Table 4 Polymer morphologies produced by spraying a solution of PS in toluene into CO_2 at 0.4°C ($\rho_{CO_2} = 0.94\,g\,ml^{-1}$)[a]

Polymer conc. (wt%)	Solution flow rate ($ml\,min^{-1}$)	Microstructure (SEM)
5	0.1	Hollow fibre with microspheres (2–3 μm) on inner wall
5	~ 1	Fibrils–beads (fused microspheres)[5] (2–3 μm)
5	3.3	Oriented fibrils, 1–3 μm diameter
8	0.1	Hollow fibre, ~ 100 μm diameter
8	2	Oriented fibrils, 1–2 μm diameter
10	0.15	Hollow fibre, ~ 100 μm diameter
10	~ 1.5	Submicrometre bicontinuous structure[5]
10	2.5	Oriented fibrils, 1–4 μm diameter

[a] Nozzle i.d. = 50 μm, length = 2.5 cm

Previously[5], experiments were performed at similar conditions, except at a flow rate of ~ $1\,ml\,min^{-1}$, which is between the above two cases (see *Table 4*). Oriented fibrils were produced, made up of fused microspheres without a skin. This morphology is intermediate between a hollow fibre with a skin and oriented fibrils. Here there

was enough time for nucleation and growth of fibrils before a skin could form. However, the shear is too low to form fibrils. Thus, fused microspheres are still present and are not completely sheared into smooth fibrils.

Dixons's earlier studies[5] also studied two flow rates for a more concentrated 10% solution. At a ΔP of 69 bar, a bicontinuous structure was formed containing submicrometre polystryene spheres interspersed with solvent voids. As the ΔP was increased to 207 bar, continuous 150 μm airy fibres were formed, composed of highly oriented 0.2–1 μm fibrils.

New results are presented for a concentration of 10% in *Table 4* at a much lower flow rate of 0.15 ml min^{-1}. A 100 μm hollow fibre with a well defined cylindrical shape was formed, which is indicative of a polymer-continuous morphology. The shell of the order of 8–10 μm is thicker than the one for a 5% solution, as expected. The higher viscosity and skin formation prevented fibril formation.

Not only did we study a lower flow rate than Dixon, but we also studied a higher flow rate of 2.5 ml min^{-1} (*Table 4*). The fibril diameters range from 1 to 4 μm. The results resembled the fibril structure formed at lower concentration, reflecting similar chain disentanglement, jet turbulence and fast mass-transfer rates. Because the concentration is well above the measured plait point, it is likely that the fibrils are polymer-continuous.

To put these results in perspective, we calculated the transition concentration C^* for this system for a temperature range of 20–30°C. Again, the intrinsic viscosity was determined from the data reported by Allcock and Lampe[27] ($K = 1.05 \times 10^{-2}$, $a = 0.72$). For a polystyrene molecular weight of 200 000, the calculated C^* is 1.7%, for a good solvent. This value is higher than the one obtained for the polyacrylonitrile solution. For the PS solutions, higher concentrations are needed to achieve similar viscosities or C^* values. For example, a 2% polyacrylonitrile solution has the same viscosity as a 5% polystyrene solution.

The Θ-solvent limit for C^* is approximately 17% polystyrene (see equation (2)). The phase separation takes place for C^* between 1.7 and 17%, in agreement with the changes in morphology from microspheres to hollow fibres reported in *Table 4*.

Finally, it is interesting to note the following similarity for the PAN–DMF and PS–toluene systems. In the PAN system, the observed transition concentration is in the range of 1.8% *versus* a value of C^* (good) of 0.6%. In the PS system, the corresponding values are 5% and 1.7% respectively. In each case the transition occurs at about $3C^*$ (good). This may suggest some similarity in the mass-transfer mechanisms in each system, although there will be some differences for an amorphous *versus* a semicrystalline polymer.

ACKNOWLEDGEMENTS

We are grateful for support from NSF (CTS-9218769), the Texas Advanced Technology Program (3658-198), and the Mexican Government through CONACYT (GLB). We thank Dr Hugo Steinfink for performing the X-ray analysis, and Roger Bonnecaze, David Dixon and Simon Mawson for helpful discussions.

REFERENCES

1 McHugh, M. A. and Guckes, T. L. *Macromolecules* 1985, **18**, 674
2 Seckner, A. J., McClellan, A. K. and McHugh, M. A. *AIChE J.* 1988, **34**, 9
3 Dixon, D. J., Bodmeier, R. A. and Johnston, K. P. *AIChE J.* 1993, **39**, 127
4 Dixon, D. J., Ph.D. Thesis, University of Texas at Austin, 1992
5 Dixon, D. J. and Johnston, K. P. *J. Appl. Polym. Sci.* 1993, **50**, 1929
6 Yeo, S. D., Lim, G. B. and Debenedetti, P. G. *Biotechnol. Bioeng.* 1993, **41**, 341
7 Randolph, T. W., Randolph, A. D., Mebes, M. and Yeung, S. *Biotechnol. Prog.* 1993, **9**, 429
8 Bodmeier, R., Wang, H., Dixon, D. J., Mawson, S. and Johnston, K. P. *Pharmaceut. Res.* in press
9 Schmitt, W. J., Preparation of finely divided powders by carrier solvent injection into a supercritical or near critical fluid, AIChE National Meeting, 1994
10 Boen, S. N., Bruch, M. D., Lele, A. K. and Shine, A. D. 'Polymer Solutions, Blends, and Interfaces' (Eds. I. Noda and D. N. Runbingh), Elsevier Science, Amsterdam, 1992, p. 151
11 Tom, J. W. and Debenedetti, P. G. *J. Aerosol Sci.* 1991, **23**, 555
12 Dixon, D. J., Luna-Bárcenas, G. and Johnston, K. P. *Polymer* 1994, **35**, 3998
13 Yeo, S. D., Debenedetti, P. G., Radosz, M. and Schmidt, H. W. *Macromolecules* 1993, **26**, 6207
14 Napper, D. H. 'Polymeric Stabilization of Colloidal Dispersions', Academic Press, New York, 1983
15 Sanchez, I. C. 'Encyclopedia of Physical Science and Technology', Vol. II, Academic Press, New York, 1992
16 Ziabicki, A. 'Fundamentals of Fibre Formation', Wiley, Chichester, 1976
17 Koenhen, D. M., Mulder, M. H. V. and Smolders, C. A. *J. Appl. Polym. Sci* 1977 **21**, 199
18 Yilmaz, L. and McHugh, A. J. *J. Appl. Polym. Sci.* 1986, **31**, 997
19 Pinnau, I., Ph.D. Thesis, University of Texas at Austin, 1991
20 Bulte, A., Ph.D. Thesis, Twente University, The Netherlands, 1994
21 Lefebvre, A. H. 'Atomization and Sprays', Hemisphere, New York, 1989
22 Bird, R. B., Armstrong, R. C. and Hassager, O. 'Dynamics of Polymeric Liquids', Vol. 1, 'Fluid Mechanics', Wiley, New York, 1977
23 McHugh, A. J. and Silebi, C. *Polym. Eng. Sci.* 1976, **16**, 158
24 Strathmann, H. and Kock, K. *Desalination* 1977, **21**, 241
25 Berens, A. R. and Huvard, G. S. *Am. Chem. Soc., Symp. Ser.* 1989, No. 406
26 Rinaudo, M. *J. Appl. Polym. Sci., Appl. Polym Symp.* 1993, **52**, 11
27 Allcock, H. R. and Lampe, F. W. 'Contemporary Polymer Chemistry', 2nd Edn., Prentice Hall, Englewood Cliffs, NJ, 1990